Preprint ISS - 8 - 1997 (December, 1997)
Institute of Space Sciences, Bucharest, Romania

FRAGMENTATION AND MULTIFRAGMENTATION OF 10.6A GeV GOLD NUCLEI

EMU01-Collaboration

M. I. Adamovich[13], M. M. Aggarwal[4], Y. A. Alexandrov[13], R. Amirikas[17], N. P. Andreeva[1], S. K. Badyal[8], A. M. Bakich[17], E. S. Basova[18], K. B. Bhalla[7], A. Bhasin[8], V. S. Bhatia[4], V. Bradnova[6], V. I. Bubnov[1], X. Cai[20], I. Y. Chasnikov[1], G. M. Chen[2], L. P. Chernova[19], M. M. Chernyavsky[13], S. Dhamija[4], K. El Chenawi[11], D. Felea[3], S. Q. Feng[20], L. N. Filippova[1], A. S. Gaitinov[1], E. R. Ganssauge[12], S. Garpman[11], S. G. Gerassimov[13],A. Gheata[3], M. Gheata[3], J. Grote[15], K. G. Gulamov[19], S. K. Gupta[7], V. K. Gupta[8], M. Haiduc[3], D. Hasegan[3], U. Henjes[12], B. Jakobsson[11], L. Just[21], E. K. Kanygina[1], S. P. Kharlamov[13], A. D. Kovalenko[6], S. A. Krasnov[6], V. Kumar[7], V. G. Larionova[13], I. A. Lebedev[1], Y. X. Li[5], L. S. Liu[20], Z.G. Liu[5], J. J. Lord[15], N. S. Lukicheva[19], Y. Lu[2], S. B. Luo[10], L. K. Mangotra[8], I. Manhas[8], I. S. Mittra[4], A. K. Musaeva[1], S. Z. Nasyrov[18], V. S. Navotny[19], J. Nystrand[11], G. I. Orlova[13], I. Otterlund[11], L. S. Peak[17], N. G. Peresadko[13], N. V. Petrov[18], V. A. Plyushchev[14], W. Y. Qian[20], Y. M. Qin[10], R. Raniwala[7], N. K. Rao[8], J. T. Rhee[16], M. Roeper[12], V. V. Rusakova[6], N. Saidkhanov[19], N. A. Salmanova[13], A. M. Seitimbetov[1], R. Sethi[4] , B. Singh[7], D. Skelding[15], V. I. Skorobogatova[1], K. Söderström[11], E. Stenlund[11], L. N. Svechnikova[19], T. Svensson[11], A. M. Tawfik[12], V. Topor Pop[3], M. I. Tretyakova[13], T. P. Trofimova[18], U. I. Tuleeva[18], B. P. Tursunov[18], Vani Vashisht[4], S. Vokal[9], J. Vrlakova[9], H. Q. Wang[11,20], S. H. Wang[2], X. R. Wang[20], J. G. Wang[17], Z. Q. Weng[5], R. J. Wilkes[15], C. B. Yang[20], Z. B. Yin[20], L. Z. Yu[20], I. S. Zgura[3], D. H. Zhang[10], P. Y. Zheng[2], S. I. Zhokhova[19], D. C. Zhou[20].

1 High Energy Physics Institute, Almaty, Kazakstan
2 Institute of High Energy Physics, Academia Sinica, Beijing, China
3 Institute of Space Sciences, Bucharest, Romania
4 Department of Physics, Panjab University, Chandigarh, India
5 Department of Physics, Hunan Education Institute, Changsha, Hunan, China
6 Laboratory of High Energies, Joint Institute for Nuclear Research (JINR), Dubna, Russia
7 Department of Physics, University of Rajasthan, Jaipur, India
8 Department of Physics, University of Jammu, Jammu, India
9 Department of Nuclear Physics, University of P. J. Safarik, Kosice, Slovakia
10 Department of Physics, Shanxi Normal University, Linfen, Shanxi, China
11 Department of Physics, University of Lund, Lund, Sweden
12 F.B. Physik, Philipps University, Marburg, Germany
13 P.N. Lebedev Institute of Physics, Moscow, Russia
14 V.G. Khlopin Radium Institute, St. Petersburg, Russia
15 Department of Physics, University of Washington, Seattle, Washington, U.S.A.
16 Department of Physics, Kon-kuk University, Seoul, Korea
17 School of Physics, University of Sydney, Sydney, Australia
18 Lab. of Relativistic Nuclear Physics, Institute of Nuclear Physics, Tashkent, Uzbekistan
19 Lab. of High Energies, Physical-Technical Institute, Tashkent, Uzbekistan
20 Institute of Particle Physics, Hua-Zhong Normal University, Wuhan, Hubei, China
21 Institute of Experimental Physics, Slovac Academy of Science, Kosice, Slovakia.

Abstract : We present the results of a study performed on the interactions of 10.6A GeV gold nuclei in nuclear emulsions. In a minimum bias sample of 1311 interactions, 5260 helium nuclei and 2622 heavy fragments were observed as Au projectile fragments. The experimental data are analyzed with particular emphasis of target separation interactions in emulsions and study of critical exponents. Multiplicity distributions of the fast-moving projectile fragments are investigated. Charged fragment moments, conditional moments as well as two and three - body asymmetries of the fast moving projectile particles are determined in terms of the total charge remaining bound in the multiply charged projectile fragments. Some differences in the average yields of helium nuclei and heavier fragments are observed, which may be attributed to a target effect. However, two and three-body asymmetries and conditional moments indicate that the breakup mechanism of the projectile seems to be independent of target mass. We looked for evidence of critical point observable in finite nuclei by study the resulting charged fragments distributions. We have obtained the values for the critical exponents γ, β and τ and compare our results with those at lower energy experiment (1.0A GeV data). The values suggest that a phase transition like behavior, is observed .

1 Introduction

The experiment to be described here examines the breakup of relativistic gold nuclei when they interact with the target nuclei in nuclear emulsions. The fragments produced are readily identified in the emulsions. Specific attention in this paper is directed towards the multiply charged fragments that are produced. Some reports on the main characteristics of the interactions have been published previously [1]-[10].

Depending upon the target - projectile combination and the incoming projectile energy, the excited piece of nuclear matter decays predominantly by the emission of nucleons, deuterons, tritons, helium nuclei and charged particles with $3 \leq Z \leq 30$ commonly known as intermediate - mass fragments (IMF's) and fragments of very heavy charge $Z \geq 31$. To understand the dynamics involving the formation of helium, IMF's and other multi-fragments in its final state, numerous experiments have been performed at low, intermediate and high energies, in both p-nucleus and nucleus-nucleus reactions [11]-[29].

The experiment to be described here examines the breakup of relativistic gold nuclei when they interact with the target nuclei in nuclear emulsions. The relative yields of the different types of fragment and the relationships between them are measures of processes that occur during the breakup of the excited nuclear remnants. We will study some relationships and compare with those observed in others experiments. In this paper we shall present a systematic study on the target and projectile fragmentation of the ^{197}Au - induced emulsion interactions at $10.6A\ GeV$ from the BNL Alternating Gradient Synchrotron (AGS).

Competing models suggest different decay mechanism and experiments have yet to discriminate between several theoretical scenarios which range from the sequential decay of the compound nucleus [30, 31] to statistical nuclear models [32, 33] and percolation models [34, 35].

It has been stressed out by Campi [36] that the moments of the charge distributions provide a test of the suggestion that multifragmentation can be described in terms of percolation theory. If there is some critical behavior in the breakup of the nuclei, such as a liquid - gas phase transition, then some events should have values of normalized moments much larger than the average. For the low energy gold interactions [26] there was a wide range of values and strong and approximately linear correlations between the different normalized moments, although it was not possible to conclude that then was a phase transition. Also EOS collaboration [27] have reported some of their results

from the analysis of 1.0A GeV gold nuclei fragmenting in a carbon target. In their analysis of 9716 interactions they used the methods developed for determining percolation critical exponents to extract the values of specific exponents for nuclear matter from the moments of the fragment charge distribution.

However, one of the main problem encountered in interpreting the results from nuclear emulsion experiments is the non-homogeneous composition of the emulsion, which contains both light (H, C, N, O) and heavy (Ag, Br) target nuclei. Critical remarks about using minimum biased samples for studing critical behavior have been expressed [16]. It has been argued that in emulsion experiments the mixture between emission sources, both with respect to origin and size, should be a severe shortcoming for collisions from few hundreds of MeV/nucleon up to several GeV/nucleon [16].

Therefore one of the main objective of this paper is to present a detailed analysis of specific measured quantities for multifragmentation phenomenon for a larger sample of these interactions of gold nuclei, with special emphasis on the inclusive interactions with separated light and heavy target nuclei.

Recently EMU01-Collaboration [10] using a statistical analysis based on event by event charge distributions, showed that a population of sub-critical, critical and supercritical events was observed among peripheral collisions, but the study has been limitted only to critical exponent γ, which in some papers [27] is claimed to show little sensitivity to the system under investigation .

KLMM Collaboration [23] has also looked for evidence of phase changes in the description of multifragmentation at 10.6A GeV, but their results are significantly inconsistent with those reported at lower energies, suggesting that percolation theory becomes a less satisfactory representation of the breakup for these high energy interactions than it was at lower energies.

Therefore it will be of great interest to repeat such analysis at the same energy and study the values for all critical exponents, using the same methods.

2 Experimental Details

Several stacks of electron sensitive, NIKFI BR-2 emulsions, of dimension 10 X 10 X 0.06 cm^3 have been exposed to a $10.6A\,GeV$ ^{197}Au beam at BNL synchrotron (experiment E863). The sensitivity of emulsion was about 30 grains per unit length of 100 μm for singly charged particles with minimal ionization.

Primary interactions were found by along - the track double scanning : fast in the forward direction and slow in the backward direction. Fast scanning was made with a velocity excluding any discrimination of events in the number of heavily ionizing tracks, slow scanning was carried out to find events, if any, with little changed and unbiased projectile nucleus. This analysis immediately resulted in a determination of the mean free path (mfp) for interactions. The measured mean free path $\lambda = 4.99 \pm 0.16\ cm$ agreed well with KLMM - collaboration result $\lambda = 4.7 \pm 0.2\ cm$ [23] and an approximation of measured cross-sections on various nuclei and targets $\lambda = 4.6\ cm$ [38].

In each event the polar angles θ and azimuthal angles φ were measured. Depending on ionization, all tracks emitted from the interaction vertices were classified according to the commonly accepted emulsion experiment terminology :

1)Shower, or **s** - particles - singly charged particles with a velocity $\beta \geq 0.7$; they, mainly, consist of produced particles and singly charged fragments.

2)Grey, or **g** - tracks, whose ionization (the number of grains per unit length) correspond to protons with momentum $0.2 \leq p \leq 1\ GeV/c$; they consist, mainly of protons knocked

- out from the target nucleus during the collision with a few percent admixture of π mesons with momentum $60 \leq p \leq 170\ MeV/c$.

3)Black, or **b** - tracks - mostly, protons with $p \leq 0.2\ GeV/c$ and multiply charged target fragments. They have a range of $< 3\ mm$.

4) Fragments of projectile nucleus - particles with $Z \geq 2$. Fragments with $Z = 2$ are identified by visual inspection of tracks, their ionization is constant and equal to $g/g_0 \approx 4$, g_0 - ionization due to relativistic particle (minimal ionization).

To determine charge of fragments with $Z \geq 3$, the density was measured of δ electrons on length no less than 10 mm ; the beam track and track with $Z = 2$ were chosen as tracks for calibrating. The accuracy of charge measurement was for $Z < 10$, ± 1 for $10 \leq Z < 28$, ± 2 for $28 \leq Z < 40$ and ± 3 for $Z \geq 40$ in units of charge.

Grey and black tracks amount the group of heavily ionizing tracks $N_h = N_g + N_b$.

In each event, the number of produced particles, π mesons (N_π) have been also determined.

A number of 1311 inelastic interactions were obtained after excluding from the ensemble events those of electromagnetic origin and pure elastic scattering. Others details on experiment especially on charge fragment measurements and errors, have been recently published [10].

3 Projectile breakup

3.1 Average multiplicity of fast - moving particles.

The difference between the projectile and the target spect-ator fragments is easy to make. Projectile fragments and shower particles are very energetic and they are distributed in a forward narrow cone. The angle of this cone is $< \theta_0 > = 16.4$ mrad and it can be found from the pseudorapidity distribution of the shower particles.

The target fragments are observed as highly ionizing particles, isotropically distributed. They can be **black** particles which are essentially evaporation fragments from the target, with $R < 3\ mm$, or **gray** particles which are knock-out protons or slow mesons with $R > 3\ mm$.

The breakup of the projectile can be characterized in terms of the numbers, N_F - and charges , Z_F, of the fragments with $Z \geq 3$, that are emitted ; the number N_α, of alpha particles emitted and the numbers N_{prot}, of protons released and available to interact, where from charge balance we can write :

$$N_{prot} = Z_{Au} - \sum_{Z_F \geq 3} N_F * Z_F - 2 * N_\alpha \tag{1}$$

We obtain the bound charge by Z_{bound} ,by :

$$Z_{bound} = \sum_{Z \geq 2} n(Z) * Z \tag{2}$$

where $n(Z)$ is the multiplicity of the projectile fragments with $Z \geq 2$.

In Table I , we display results of the present investigation of the average multiplicities $< N_{prot} >$, $< N_\alpha >$, and $< N_F >$ of the fragments with $Z = 1$, $Z = 2$, and $Z \geq 3$, respectively, for the ^{197}Au ions.

Also a comparison with the results of Cherry et al. [23] and those of Singh and Jain [22] at 10.6A GeV are given. A good agreement with both experiments is obtained for $< N_{prot} >$ and $< N_{\alpha} >$, but a slight difference is remarked for mean number of projectile fragments with $Z \geq 3$.

Table 1: The average multiplicity of projectile fragments with $Z = 1$, $Z = 2$, *and* $Z \geq 3$ emitted in the ^{197}Au - induced reactions in emulsions at 10.6A GeV.

Beam	Energy (AGeV)	$< N_{prot} >$	$< N_{\alpha} >$	$< N_F >$	Ref.
^{197}Au	10.6	28.48 ± 0.81	4.63 ± 0.13	2.01 ± 0.06	[22]
^{197}Au	10.6		4.53 ± 0.13	1.91 ± 0.06	[23]
^{197}Au	10.6	28.44 ± 0.64	4.51 ± 0.08	2.37 ± 0.03	This work

The numbers of fragments emitted from individual interactions can be compared by looking at the distributions of the numbers of events with a given number of fragments divided by the total number of events, the fractional yield. These fractional yields for fragments, those with $Z \geq 3$ (Fig. 1a), for alpha particles (Fig. 1b), for heaviest fragments (Fig. 1c) and for numbers of released protons (Fig. 1d) are compared in Figure 1 with the published results of KLMM collaboration [23, 24]. It appears that these yields are nearly identical, although some differences appear especially for heaviest fragment and number of proton released.

The experimental spectra for number of released protons (Fig. 2a) and number of produced pions (Fig. 2b) as well as their correlation with number of mesons (Fig. 2c) and the number of heavily ionizing tracks N_h (Fig. 2d) are given in Figure 2. As would be expected, there is a strong correlation between the number of proton released and the number of pions produced - there is a rather well defined upper bound to the number of pions N_{π} for a given number of proton released N_{prot}. Fig. 2d shows that interactions with light target nuclei, those with $N_h \leq 7$, never results in a copious pion production. For $N_h > 8$, where the target must have been a AgBr nucleus, N_{π} appears to be almost independent of N_h.

It is interesting to note that our data set for ^{197}Au do not give any evidence of the occurrence of binary fission in the charge range of $35 \leq Z \leq 45$ [9], although a significant enhancement of the fission events was observed at lower energies with the ^{197}Au projectile, as reported in Ref. [26].

3.2 Correlation between N_{α} and N_F

Broad characteristics of the projectile fragmentation can be explored through the correlation between the multiplicity of helium particles N_{α} and heavier fragments N_F . Such a correlation is given in Table 2 for the ^{197}Au data . From Table 2 one can see that the number of pure central interactions, in which the projectile has disintegrated completely into singly charged fragments with no emission of heavier fragments, is very small (≈ 1 %). More than 20 % of the events have $N_{\alpha} = 0$ and $N_F = 1$. Only 2.5 % of the total number of interactions is found with $N_F \geq 5$ and $0 \leq N_{\alpha} \leq 10$. On the other hand, only 2.1 % of the total umber of collisions is observed with $N_F < 5$ and $N_{\alpha} > 10$. No event is observed with $N_F \geq 8$ and $N_{\alpha} > 10$. The maximum number of fragments with $Z \geq 3$ in our sample is $N_F = 8$ and that of fragments with $Z \geq 2$ is $N_{\alpha} + N_F = 21$.

Table 2: Characteristics of projectile fragmentation of the ^{197}Au beam through a correlation between the number of helium particles, N_α and the number of heavy fragments, N_F with $Z \geq 3$.

	$N_F = 0$	1	2	3	4	5	6	7	8
$N_\alpha = 0$	16	165	231	17	1	0	0	0	0
1	21	90	18	6	1	1	1	0	0
2	14	67	30	14	4	0	0	0	0
3	18	70	36	19	13	3	21	0	0
4	9	50	50	34	10	8	4	0	1
5	3	33	40	33	19	2	3	0	0
6	3	24	31	21	14	5	2	0	0
7	1	20	28	21	12	6	3	0	0
8	5	16	22	14	8	4	0	1	0
9	3	10	16	7	12	6	1	0	0
10	2	9	13	7	5	1	0	0	0
11	0	4	4	3	4	2	0	0	0
12	0	0	1	2	1	0	0	0	0
13	0	1	1	3	0	0	0	0	0
14	0	2	0	0	0	0	0	0	0
15	0	0	1	1	0	0	0	0	0
16	1	1	0	0	0	0	0	0	0

Specific correlations for mean number $< N_F + N_\alpha >$ with number of singly charged fragments (N_P) are shown in Fig. 3a. We can remark an expected linear correlation for $N_P \leq 10$ and a plateau for $N_P > 10$. Correlations with number of shower particles N_S are given in Fig. 3b, (we note that N_S does not include singly charged fragments N_P) indicate a clear change in slope for $N_S > 70$, which is due to separation of central and peripheral collisions. A *rise* and *fall* for correlations of mean number $< N_F + N_\alpha >$ with number of released proton, which are complementary to correlations with Z_{bound} (see also Fig. 5a,d) are depicted in Fig. 3c. A more complex correlations are obtained by plotting $< N_F + N_\alpha >$ as function of number of black and grey tracks (N_h) in Fig. 3d, in which we can see a different slopes for interactions with light ($N_h < 7$) and heavy nuclei ($N_h \geq 8$.

3.3 Target separation

Nuclear emulsion are a composite medium composed of AgBr, CNO and H. Certainly, they are also other nuclei in emulsions, but their concentration are too small to be taken into account. It was a difficult task to separate interactions on different classes of targets and it is impossible to find certain separation criteria that give no admixture between those classes although there are many correlations between the measurable parameters that give informations regarding the target nuclei.

The separation technique we used was based on the analysis of specific correlations between target break-up and particle production. Depending upon the target break-up, we separate the sample of 1311 interactions into three classes :

a) $N_h = 0, 1$; this class includes all Au + H interactions but also interactions with other targets.

b) $2 \leq N_h \leq 7$, containing the rest of Au + CNO interactions not included at a), but also some Au + AgBr.

c) $N_h > 7$, including only interactions with AgBr.

An additional relation that give some target separation for a) events is based on the distribution of the number of shower particles with $\theta > \theta_0$. Events with no black or gray tracks include most of the H interactions, but also the most central events with CNO and AgBr. The distribution of the shower particles for these events indicates the limit of no more than about 40 relativistic particles with $\theta > \theta_0$ emitted from Au + CNO interactions. The separation between H and CNO peaks give an admixture of less than 10 % for this class of events.

For $N_h = 1$ we analyzed separately elastic interactions from a kinematic approach. Knowing the emission angles for the black track and the recoiled gold nucleus we could compute the range-momentum ratio for most of the elastic events. This ratio is highly dependent on the target size and it's very useful in order to separate elastic interactions with CNO from those with AgBr. For elastic interactions with hydrogen nuclei, the recoil proton appear most often as a gray track. The number of shower particles for inelastic interactions with $N_h = 1$ indicates that AgBr events are for $N_{s'} > 40$.

Class b) events were separated by plotting the number of shower particles against N_h. The separation between CNO from AgBr populations is given by :

$$N_{s'} < 175 - 14.5 \cdot N_h \tag{3}$$

where, $N_{s'} = N_s + N_P$.

The reason we took the limit $N_h > 7$ for class c) events was that 8 target tracks for an oxygen nucleus correspond to a total charge break-up, reasonable to assume that at least one of the released target protons become a relativistic particle.

We plotted the distributions of the number of α particles and PF's for the interactions of gold nuclei with HCNO and AgBr targets in Figure 4. We can see in Fig. 4a that the emission of α particles is enhanced for interactions with heavy targets, the distribution being shifted to the right. However the distributions of heavy fragments in Fig. 4b show the same behavior for the two samples.

The correlations between the mean number of emitted alpha's and fragments and the total bound charge are depicted in Fig. 4c and Fig. 4d. We can see that for peripheral events corresponding to $Z_{bound} > 50$ the emission of alpha's and fragments have the same behavior both for light and heavy emulsion targets. However α particle emission is suppressed almost down to zero when centrality is increasing, especially for HCNO interactions. The difference between the two samples for PF's is not so obvious. Nevertheless we can notice some decrease of the mean number of fragments for HCNO compared to AgBr in semi-central events.

4 Specific Correlations for Multifragmentation

4.1 Correlation between some observable and Z_{bound}.

The parameter Z_{bound}, which was defined by Hubele et al., [19] is related to the size of the projectile spectator and the energy deposited in a given collision can also be explored through Z_{bound}. Z_{bound} is always larger than or equal to Z_{max}.

The heaviest fragment charge in each collision, Z_{max}, provides useful information on the exit channel of that collision. Fig. 5a shows a scatter plot of the correlation between Z_{max} and Z_{bound}

for individual events of the ^{197}Au data. We remark that most of the data points are situated below the diagonal, that means that Z_{bound} is always larger than or equal to Z_{max} . Also in the peripheral collisions, the largest fragment contains most of the total bound charge and in such reactions Z_{max} may be identified as the heavy residue of the beam nucleus after evaporation. For the central events, we observe that Z_{max} becomes a smaller fraction of Z_{bound} . This plot also confirms that symmetric fission is a very rare kind of events.

In Fig. 5b we give the variation of mean value of $< Z_{max} > /Z_{beam}$ as a function of Z_{bound} for the ^{197}Au data. A sharp rise of this ratio can be seen from Fig. 5b for $Z_{bound} \approx 40 - 79$. For $Z_{bound} \approx 2 - 40$ the rise is rather slow. This plot give some information into the degree of breakup of the projectile nucleus.

In Fig. 5c we plot the average multiplicity distributions of alpha particles $< N_\alpha >$ and in Fig. 5d the mean number of intermediate - mass fragments (IMF's) with $3 \leq Z \leq 30$ as a function of Z_{bound} for ^{197}Au projectiles. Our experimental data confirm, the so called "rise and fall" of the multi-fragment emission .

4.2 Charged fragment asymmetries

In this chapter, we investigate the charge asymmetry between the largest fragments (Z_{max}) and the second largest Z_{FM2} fragment in an event, using the two body relative asymmetry R_{AS}, defined as [19] :

$$R_{AS} = \frac{Z_{max} - Z_{FM2}}{Z_{max} + Z_{FM2}} \tag{4}$$

Only fragments with $Z \geq 2$ are included.

Also R_{AS1}, the asymmetry between the second largest Z_{FM2} and third largest Z_{FM3} in an event is obtained by :

$$R_{AS1} = \frac{Z_{FM2} - Z_{FM3}}{Z_{FM2} + Z_{FM3}} \tag{5}$$

We can also investigate the breakup process in a more qualitative manner through another parameter known as three body asymmetry [19] as :

$$R_{AS2} = \frac{\sqrt{(DFA)^2 + (DFB)^2 + (DFC)^2}}{\sqrt{6} < Z >} \tag{6}$$

where :

$$DFA = Z_{max} - < Z >$$
$$DFB = Z_{FM2} - < Z >$$
$$DFC = Z_{FM3} - < Z >$$

with :

$$< Z >= \frac{1}{3}(Z_{max} + Z_{FM2} + Z_{FM3}) \tag{7}$$

The parameter R_{AS2} has a maximum near unity when there is heavy residue of the projectile spectator and has a zero value when the projectile fragments of equal size are emitted in the collisions.

For the analysis of two body asymmetries given by Eq. (4) and Eq. (5) , we have selected the events with at least three fragments of $Z \geq 2$.

In Fig. 6a and Fig. 6b, we plot a correlation between mean value of ratio $< R_{AS} >$ and $< R_{AS1} >$ respectively with Z_{bound} for ^{197}Au data. The ratio $< R_{AS} >$ decrease monotonically from its maximum value ≈ 0.9 to almost zero as one approaches from extremely peripheral toward more violent collisions. The ratio $< R_{AS1} >$ rises linearly with Z_{bound} for $Z_{bound} \leq 40$ and decreases for $40 \leq Z_{bound} \leq 79$ for these class of events selected ($N_F + N_\alpha \geq 3$) . In Fig. 6c we represent ratio $< R_{AS} >$ for IMF's and we see that the ratio remain almost constant for $20 \leq Z_{bound} \leq 60$. For $Z_{bound} > 60$ a clear leading fragments effects appear. In Fig. 6d we plot a graph of a correlation between mean value $< R_{AS2} >$ and Z_{bound}. The parameter $< R_{AS2} >$ rises almost linearly with enhancing value of Z_{bound}.

In order to observe if there is any difference in the behavior of the projectile break-up mechanisms for interactions with different targets in emulsion, we analyzed two and three-body asymmetries between the heaviest emitted fragments.

In this analysis we used together the separation criteria for H and CNO interactions in order to eliminate any possible admixture between these groups. Thus we built two samples, the first containing interactions with light (HCNO) nuclei and the second AgBr events.

In Figure 7 we plot the same parameters for interactions with light target (HCNO) (open circles) and heavy targets (Ag,Br) (full circles) as described in section 3.3.

We plotted the correlations between the mean two and three-body asymmetry ratios for interactions with light and heavy nuclei and the total bound charge. We can see in Fig. 7a that the asymmetry ratio between the first and second heavy fragments increases monotonically both for light and heavy samples from most central interactions to peripheral one ($Z_{bound} \simeq 79$). The second and third fragment asymmetry ratio (Fig . 7b) seems to be constant for semi-central and peripheral interactions, decreasing down to 0 for $Z_{bound} < 40$ when increasing the centrality.

The asymmetry ratio for IMF's (see Fig. 7c) is constant in a wide region of Z_{bound}, peaking near the value of 70 which indicate a higher asymmetry between the IMF's in peripheral interactions. The three-body asymmetry ratio plotted in Fig. 7d show an approximately linear dependence with Z_{bound} but also there is no significant difference between the two samples.

These observations point out that multifragmentation of gold nuclei at this energy does not depend on the target nucleus. Thus it doesn't matter that nuclear emulsions contain an admixture of targets from the multifragmentation mechanisms point of view.

4.3 Moments of the Charge Distribution

Multifragmentation has been considered to be one of the most important aspects of heavy - ion collisions since it has been speculated that the decay of a highly excited nuclear system might carry information about the equation of state and the liquid-gas phase transition of low density nuclear matter. The similarity between statistical multifragmentation models and percolation theory has been stressed in ref. [34, 35] The relevance of percolation ideas in nuclear fragmentation can be investigated better by examining cross relations between various moments of the fragment size distribution. We will show in this paper that experimental data have strong similarities with the predictions of percolation models.

Following Campi [36] suggestion we investigate the moments of the charge distribution of the n_Z projectile fragments (PF's) using an event-by-event based analysis. For each event, we determine the multiplicity of charged fragments, m_{PF}, and the number of charged fragments, n_Z, of nuclear

charge Z. We then consider the $i'th$ moments of this distribution :

$$M_i = \sum_Z Z^i * n_Z \tag{8}$$

where the sum is extended over all the fragments except the biggest cluster (fragment) which is being considered as the percolating cluster [39]. Physically Z_{max} corresponds to the bulk liquid in an infinite system.

The zero order moment is obtaining by taking $i = 0$ in Eq. (8) :

$$M_0 = \sum_Z n_Z \tag{9}$$

It has also been suggested [36] that the conditional moment, γ_2, which is combined from the moments M_2, M_0 and M_1 as :

$$\gamma_2 = \frac{M_2 M_0}{M_1^2} \tag{10}$$

give more selective information.

In Figure 8 the mean values of M_0 (Fig. 8a), M_1 (Fig. 8b), and M_2 (Fig. 8d) , averaged over small range of Z_{bound} for the nonzero values of the moments, are shown as function of Z_{bound} . In Fig. 8c we represent a variation of mean values of $< \gamma_2 >$ for the events with at least three charged projectile fragments with $Z \geq 2$. The value of $< \gamma_2 >$ increases rather slowly in the range of $2 \leq Z_{bound} < 50$. The maximum value of $< \gamma_2 > \approx 1.35$ at $Z_{bound} \approx 50$ and then decreases for $Z_{bound} > 50$. Some fluctuations in $< \gamma_2 >$ can be seen in this region for the ^{197}Au data. For the values of $Z_{bound} \leq 20$, $< \gamma_2 >= 1$ (events in which the projectile fragments of the same size are emitted). For the infinite nuclear system, the scaling theory of critical phenomena predicts that at the critical point γ_2 diverges at a rate that depends on the critical indices of the phase transition [36]. For a finite nuclear system, γ_2 is predicted to have a smooth behavior [36]. From Fig. 9c we remark a smooth increase of $< \gamma_2 >$ up to $Z_{bound} \approx 60$ for the ^{197}Au data. However some fluctuations appear in our ^{197}Au sample . Similar results were analyzed for ^{197}Au data at 10.6A GeV and ^{208}Pb data at 160A GeV [22]. The peak observed is due to finite size of the nuclear systems under investigation.

In Figure 9 we study the dependence of the same quantities M_0 (Fig. 9a), M_1 (Fig. 9b), M_2 (Fig. 9d) and γ_2 (Fig. 9c) function of Z_{bound} for different interactions on light targets (open circles) and heavy targets (full circles). No significant differences between the two target groups are observed.

5 Critical Exponents in Multifragmentation

5.1 Leading fragments

Fig. 10a, exhibits an area plot of the correlation between the charge of the heaviest fragment Z_{max} and the first order moment M_1 (or remaining bound charge Z_r) . This shows that there are many interactions where $M_1 > Z_{max}$ and that, even when there is a well defined leading fragment (a fragment that carries more than half of the bound charge Z_{bound}) - it is usually accompanied by appreciable other bound charge.

$$Z_{bound} = Z_{max} + M_1 = Z_{max} + Z_r \tag{11}$$

The plot of Z_{max} versus M_1, already presented in Fig. 10a shows a clear, but complex correlation, which suggest two distinct populations. This suggestion is enhanced by separating the interactions into those with ($M_1 < Z_{max}$) and without ($M_1 > Z_{max}$) leading fragment.

If the mean values of $< Z_{max} >$ are determined over small intervals of M_1, for these two classes they will appear well separated (Fig. 10c).

A similar comparison can be drawn from the correlation between the next heaviest fragment Z_{FM2} and Z_{max} in Fig. 10b. The mathematical restrictions are indicated by the dasheded lines on this plot, but it is clear that the allowed space is not uniformly populated. In particular the fission region near the apex is almost empty (see also reference [9]), in contrast to the situation seen at lower energies ([26]).

Considering the ratio R_1 for all fragments, where :

$$R_1 = \frac{Z_{max}}{M_1} \tag{12}$$

Then there is a leading fragment, as defined above , when $R_1 > 1$. We see from Fig. 10d that ratio R_1 is a strong function of Z_{bound}. Thus, while there is a well defined leading fragment when Z_{bound} is greater than 60, it is much less well defined when Z_{bound} falls to 40.

5.2 Critical Exponents

The observation of a power law behavior for the size distribution of the fragments has triggered a number of studies that have looked for evidence of *critical behavior* [27], [23], [22], [10]. These analysis consider nuclear multifragmentation as one example of a *critical phenomenon* and attempts are made to extract from the data the related critical exponents.

The EOS Collaboration [27] have reported some of their results from the analysis of 1.0A GeV gold nuclei fragmenting in a carbon target using the methods developed for determining percolation critical exponents to extract critical exponents for nuclear matter from the moments of the fragment charge distribution [28] :

We assume that the multiplicity of fragments, $m = N_F + N_A + N_{prot}$ is a linear measure of the distance from the critical point as suggested by Campi [36]. Here N_F - is multiplicity of fragments ($Z \geq 3$, N_A is multiplicity of alpha particles ($Z = 2$ and N_{prot} is the number of released protons ($N_{prot} = Z_{beam} - Z_{bound}$ with $Z_{beam} = 79$).

The region in m below the assumed critical multiplicity m_c is designated as the *liquid phase* and that above m_c as the *gas phase*. It is assumed that in the liquid phase the heaviest fragment Z_{max} is omitted in forming the moments, but is not omitted when in the gas phase [39].

Also our analysis tacitly assumes that all of the projectile-related charges are associated with multifragmentation and include in the analysis of the moments number of released protons, N_{prot} as fragments, modifying Eq. (8) and replacing M_i by M_i^*.

The critical exponents γ, β, and τ for large systems are given by the following equations in terms of the multiplicity difference, $\zeta = m - m_c$ by :

$$M_2^* \sim |\zeta^{-\gamma}| \tag{13}$$

$$Z_{max} \sim |\zeta|^{\beta} \tag{14}$$

$$n_Z \sim Z^{-\tau} \tag{15}$$

These exponents γ, β and τ are related by the equation [40] :

$$\tau = 2 + \frac{\beta}{\beta + \gamma} \tag{16}$$

We start our analysis by examining the variation of the mean values for second moments $< M_2^* >$ as a function of multiplicity m which is depicted in Fig. 11a . A relatively abrupt change in this distribution is apparent for m_c around 26, suggesting that there could be a phase change at this critical value of m_c . This values is similar to those reported by others experiments [27], [23].

Fig. 11b shows a log-log plot of mean values of second moments $< M_2^* >$ with ζ for the assumed liquid and gas phases, setting $m_c = 26$ (where log stand for natural logaritms). The clear separation between the two phases arises from the inclusion of Z_{max} in the determination of $< M_2^* >$ in the gas phase. In Fig. 11c and Fig. 11d the values are represented in a scatter plot.

If we examine over the entire available range of ζ , neither phase shows the power law behavior predicted by Eq. 13 . However, if rather narrow regions of $|\zeta|$ are selected, $5 \leq |\zeta| \leq 20$, then a good fit to such a power low can be obtained for the gas phase , with $\gamma_{gas} = 0.86 \pm 0.05$ and a reduced χ^2 of 2.94. A fair fit can also be obtained for the liquid phase, with $\gamma_{liquid} = 0.83 \pm 0.14$, reduced χ^2 of 1.44. The results are represented in Fig. 12a.

We note that the values are relatively sensitive to the range of $|\zeta|$ used, as we expected, since finite size distorsions dominate as $|\zeta| \rightarrow 0$, and signature of critical behavior vanish for large $|\zeta|$, corresponding to mean field regime. Adding two more values to those shown in Fig. 12a changes γ to $\gamma_{liquid} = 0.69 \pm 0.11$ with χ^2 of 1.56 and $\gamma_{gas} = 0.73 \pm 0.04$ with χ^2 of 4.3.

The most important results is that the values for γ_{liquid} are close to the values of γ_{gas} , which implies that the conditions for a phase change have been satisfied. No better match can be found for $m_c = 30$. In practice to estimate the uncertainties, we varied the fitting region by changing the upper and lower multiplicity limits. The overall estimated uncertainties are 14.5 %.

We continue the analysis determining the exponent β from Eq. 14 considering the liquid phase, where Z_{max} is well defined. Fig. 12b shows $\log(< Z_{max} >)$ as a function of $|\zeta|$. The value obtained for $\beta = 0.25 \pm 0.02$ with a reduced $\chi^2 = 1.56$ is in a good agreement with that of 0.29 ± 0.02 reported at 1.0A GeV [27] (see also table 3). The value obtained for an exponent is sensitive to the range of values chosen for $|\zeta|$.

The critical exponent τ in Eq. (15) can be determined from the slope of $\log(< M_3^* >)$ versus $\log(< M_2^* >)$ (see Fig. 12c) using only the gas phase [36]. Fig. 12d shows a power law fit with $\tau = 2.23 \pm 0.05$ and a reduced χ^2 of 1.51, for $3 \leq |\zeta| \leq 36$.

Our value is practically the same with the value predicted in infinite percolation models [35] or the values reported for the 1.0A GeV [27] 2.26 or the value of 2.23 calculated from our measured values of β and γ_{gas} using Eq. (16).

Reducing the range of $|\zeta|$ values used for this fit does not make any significant change in the deduced values of τ. We note that the critical exponent τ is close to 2.2 for many three-dimensional systems and thus does not permit a determination of the universality class of phase transition.

The exponent values are summarized in table 3, which also list the values from lower energies experiment [27], percolation [39], liquid-gas values [40] and the mean field limit of the liquid-gas system [41].

Table 3: Critical multiplicity and exponents for Au projectile fragmentation and other three-dimensional systems

Quantity	$\mathbf{m_C}$	γ	β	τ
Our Exper.	26	0.86 ± 0.05	0.25 ± 0.02	2.23 ± 0.05
EOS Exper.[27]	26 ± 1	1.40 ± 0.1	0.29 ± 0.02	2.14 ± 0.06
Percolation [39]		1.8	0.41	2.18
Liquid - gas mean field [41]		1.0	0.50	2.33
Liquid-gas [40]		1.23	0.33	2.21

We note that the values of γ, β *and* τ obtaining using this method obey the scaling relation, Eq. (16). By varying the fitted region, we have obtained exponents which differ by as much as 15 %. We can take this to be a measure of the uncertainty in their values. It is significant that the values for β and γ are different from either the percolation or the mean field values. Also we can remark that γ exponent is different from those of nominal fluids and depends on energy.

6 Conclusions

In the present work we have studied, the properties of the projectile associated particles emitted in interactions of the ^{197}Au ions accelerated at an energy of $10.6A\ GeV$ obtained from the BNL AGS.

The average multiplicities of the fast - moving projectile particles such as $< N_\alpha >$, $< N_F >$, $< N_{prot} >$ seem to depend upon the mass of the target. The majority of the multiply charged fragments are helium nuclei, while the majority of those fragments with $Z \geq 3$ are light. The multifragment emission is a dominant reaction channel as observed when the distributions of $< N_\alpha >$, $< N_{IMF} >$ are represented as function of Z_{bound}. These distributions are peaked at $Z_{bound} \approx 35 - 40$ and shows slight dependence on the target mass.

Nuclear emulsion detectors provide an excellent tool to study the global characteristics of nucleus-nucleus interactions since they allow a simultaneous investigation of the processes of nuclear fragmentation and multiple particle production and allow a study of the correlations between these processes.

Even if the emulsion detector contains different targets, multifragmentation, when expressed in terms of Z_{bound} , appears to be relatively insensitive to the nature of the target and the results can be compared with those from studies using pure targets.

An analysis of the moments M_0 , M_1 and M_2 as well as conditional moments such as γ_2 also proves that the breakup mechanisms has no dependence on the target size and a broad peak in the γ_2 - Z_{bound} relation shows that the nuclear systems employed in the present investigation induced a finite size effect.

Two and three body asymmetries are explored through the distributions of $< R_{AS} >$,$< R_{AS1} >$ and $< R_{AS2} >$ as a function of Z_{bound} . Within statistical errors, the distributions shows almost similar behavior on different target which indicates that the breakup mechanism has no dependence on target mass.

A study of multiplicities suggest that there could be a phase change in the residual nucleus that depends on the multiplicity of the charge fragments, in a manner similar to that predicted by theories such as percolation that describe the process of multifragmentation.

Our analysis for a critical point and a phase change based on our high energy data give results which are consistent with the analysis reported for the low energy results. The presence of a critical point is well established from our data. Comparison with percolative and liquid-gas systems show remarkable similarities. However, some essential differences on values of critical exponents are pointed out.

To further characterize this phenomenon, we must determine whether the fragmenting system is thermalized and if so its temperature and density [42], and also whether the multiplicity is proportional to temperature. Some results have been published recently [43, 44].

7 Acknowledgements

Financial support from the Swedish Natural Science Research Council, the Int. Sci. Foundation and the Russian Foundation of Fundamental Research, the German Federal Minister of Research and Technology, the University Grants Commission ANR the Department of Science and Technology of the Government of India, the National Natural Science Foundation of China, the Foundation of the State Education Commission of China, the Grant Agency for Science at the Ministry of Education of Slovak Republic and the Slovak Academy of Sciences and the US Department of Energy, the German Academic Exchange Service (DAAD), the Australian Research Council, Kon-Kuk University Research Fund, the Romanian Ministry of Research and Technology and the National Science Foundation are cordially and gratefully acknowledged.

References

[1] EMU01 Collaboration, M. I. Adamovich et al., Phys. Rev. Lett. **69,** 745 (1992)

[2] EMU01 Collaboration, M. I. Adamovich et al., Nucl. Phys., **B388,** 3 (1992)

[3] EMU01 Collaboration, M. I. Adamovich et al., J. Phys. G ; Nucl. Part. Phys., 2035 (1993)

[4] EMU01 Collaboration, M. I. Adamovich et al., Z. Phys. **C65**, 421 (1995)

[5] EMU01 Collaboration, M. I. Adamovich et al., Phys. Lett. **B363,** 230 (1995)

[6] EMU01 Collaboration, M. I. Adamovich et al., Nucl. Phys. **A590**, 597c (1995)

[7] EMU01 Collaboration, M. I. Adamovich et al., Phys. Lett. **B352**, 472 (1995)

[8] EMU01 Collaboration, M. I. Adamovich et al., J. Phys. G ; Nucl. Part. Phys., 22 (1996)

[9] EMU01 Collaboration, M. I. Adamovich et al., Proceedings of 25th International Cosmic Ray Conference, Durban (29 July - 10 August, 1997) **HE 1.1.13**, Volume **6**, 21 (1997)

[10] EMU01 Collaboration, M. I. Adamovich et al., Eur. Phys. J. **A1**, 77 (1998)

[11] P. A. Gorichev, O. V. Lozhkin, N. A. Perfilov and Yu. P. Yakovlev, Sov. Phys. JETP **41**, 327 (1961)

[12] J. E. Finn et al., Phys. Rev. Lett. **49**, 1321 (1982)

[13] R. W. Minich et al., Phys. Lett. **118B**, 458 (1982)

[14] B. Jakobsson, G. Jönsson, B. Lindkvist and A. Oskarsson, Z. Physik **A307**, 293 (1982)

[15] J. W. Harris et al., Nucl. Phys. **A471**, 241 (1987)

[16] B. Jakobsson et al., Nucl. Phys. **A509**, 195 (1990)

[17] R. T. de Souza et al., Phys. Lett. **B268**, 6 (1991)

[18] Y. D. Kim et al. Phys. Rev. Lett. **63,** 494 (1989) ; E.Piasecki et al., *ibid.* **66,** 1291 (1991), D. R. Browman et al., *ibid.* **67,** 1527 (1991)

[19] C. A. Ogilvie et al., Phys. Rev. Lett., **67,**1214 (1991) ; K. Hagel et al., *ibid.,* **68,** 2141 (1992) ; J. Hubele et al., Z. Phys. **340**, 263 (1991) ; J. Hubele et al., Phys. Rev. **C46**, R1577 (1992) ; P. Kreutz et al., Nucl. Phys. **A556,** 672 (1993)

[20] P. L. Jain, G. Singh and A. Mukhopadhyay, Phys. Rev. **C50,** 1085 (1994) ; G. Singh and P. L. Jain , *ibid.* **49**, 3320 (1994)

[21] G. Rusch, W. Heinrich, B. Wiegel, E. Winkel and J. Dreute, Phys. Rev. **C49**, 901 (1994)

[22] G. Singh and L. P. Jain , Phys. Rev. **C54**, 3185 (1996)

[23] M. L. Cherry et al., Phys. Rev. **C52,** 2652, (1995)

[24] C. J. Waddington, Int. J. Phys. **E2**, 739 (1993)

[25] D. G. Enteria et al. , Phys. Rev. **C52,** 3179 (1995)

[26] C. J. Waddington and P. S. Freier, Phys. Rev. **C31**, 388 (1985)

[27] M. Gilkes et al., Phys. Rev. Lett. **73**, 1590 (1994) ; N. T. Porile (for EOS Collaboration), Proc. of the 7 th Int. Conf. on Nuclear Reaction Mechanisms, edited by E. Gadioli, Varena, June 6-11, 1994, p555-564

[28] J. B. Elliot et al., Phys. Rev. **C49**, 3185 (1994)

[29] H. G. Ritter et al., in Proceedings of the 5th Interactions Conferences on Nucleon - Nucleon Collisions, 1994, LBL Report No 36105, 1994

[30] W. A. Friedman, Phys. Rev. **C42**, 667 (1990)

[31] R. J. Charity et al., Nucl.Phys. **A483**, 371 (1988)

[32] D. H. E. Gross, Rep. Prog. Phys. **53**, 605 (1990) and H.R. Jaqaman and D. H. E. Gross, Nucl. Phys. **A524,** 321 (1991)

[33] J. Bondorf et al., Nucl. Phys. **A444,** 460 (1985)

[34] W. Bauer, Phys. Rev. **C38**, 1297 (1988) ; W. Bauer et al., Annu. Rev. Nucl. Sci. **42**, 77 (1992) ; J. D. Desbois, Nucl. Phys. **A466**, 724 (1987)

[35] D. Stauffer, Phys. Rep. **54**, 1 (1979) ; X. Campi, Phys. Lett. **B208**, 351 (1988) ; J. Phys. **19**, 917 (1986) ; X. Campi and H. Krivine, Z. Phys. **A344**, 81 (1992)

[36] X. Campi , J. Phys. **A 19,** L917 (1986) ; *ibid* J. Phys. Math. Gen. **19**, 917 (1986) ; *ibid* Phys. Lett. **B208**, 351 (1988)

[37] K. Werner , Phys. Lett., **B208**, 520 (1988)

[38] W. R. Binns et al., Phys. Rev. **C36** , 1870 (1987)

[39] D. Stauffer and A. Aharony, Introduction to Percolation Theory, second edition (Taylor and Francis, London, 1992)

[40] H. E. Stanley, Introduction to Phase Transitions and Critical Phenomena (Oxford University Press, 1971)

[41] H. B. Callen, Thermodynamics and Introduction to Thermostatistics, second edition (John Wiley and Sons, New York, 1985)

[42] *Nuclear Physics in Europe : Highlights and Opportunities*, edited by J. Vervier, Juha Äystö, H. Doubre, S. Gales, G. Morrison, G. Ricco, D. Schwalm and G. E. Körner , NuPECC REPORT, December 1997, *Nucleus-Nucleus Collisions and the Phase Transitions of Nuclear Matter*, p 55

[43] EMU01 Collaboration, M. I. Adamovich et al., Z. Physik. **A358**, 337 (1997)

[44] EMU01 Collaboration, M. I. Adamovich et al., Z. Physik. **A359**, 277 (1997)

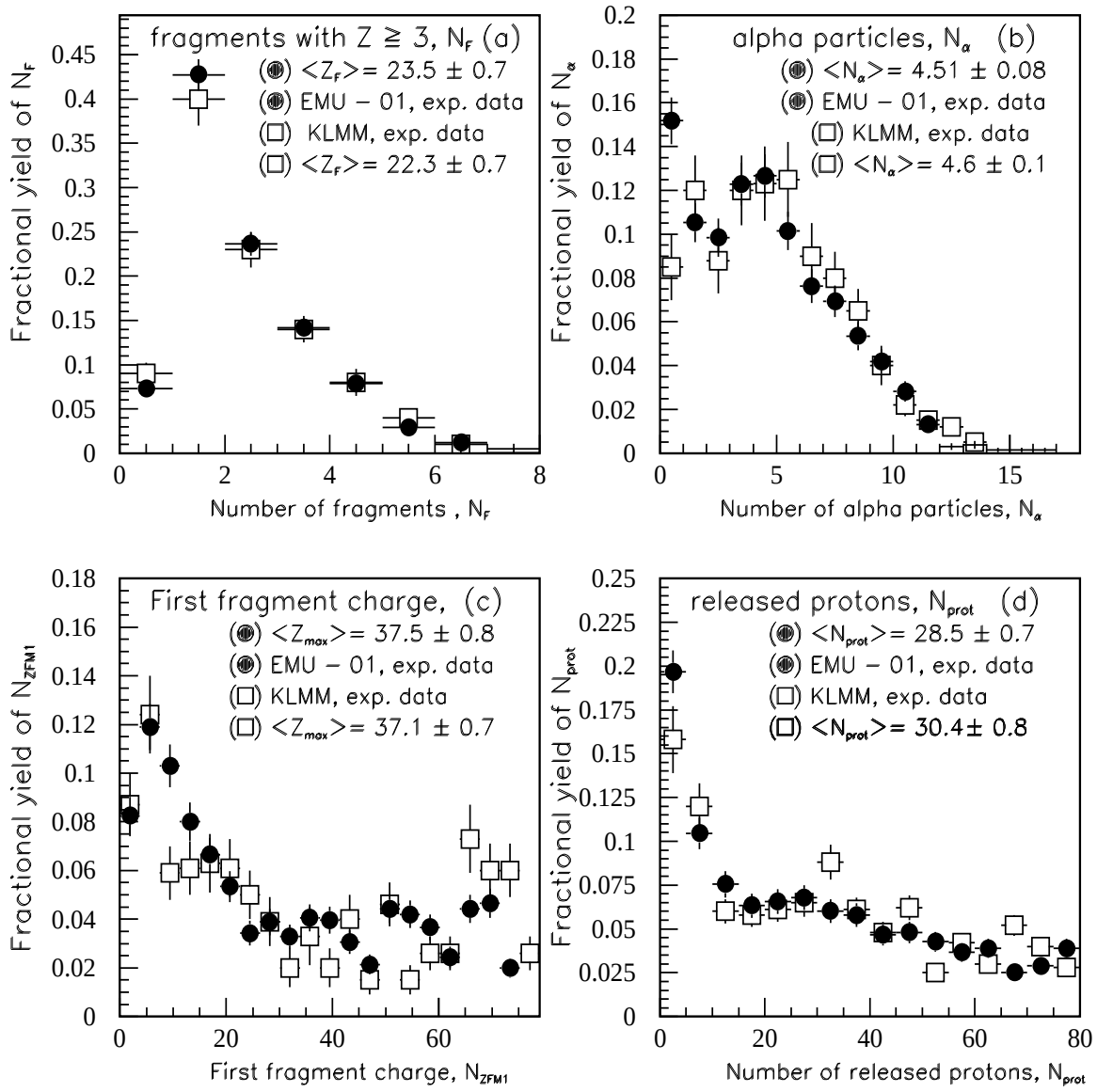

Figure 1: Part (a) - Fractional yields of fragments with $Z \geq 3$ observed in the two experiments ; EMU-01 data (full circles) and KLMM data (open squares). Part (b) - Fractional yields of alpha particles in the two experiments as a function of alpha particles emitted from an interaction. Part (c) - Fractional yields of the heaviest fragments in the same experiments as a function of the charge of the fragment. Part (d) - Fractional yields of released protons as a function of the numbers of protons released from an interaction.

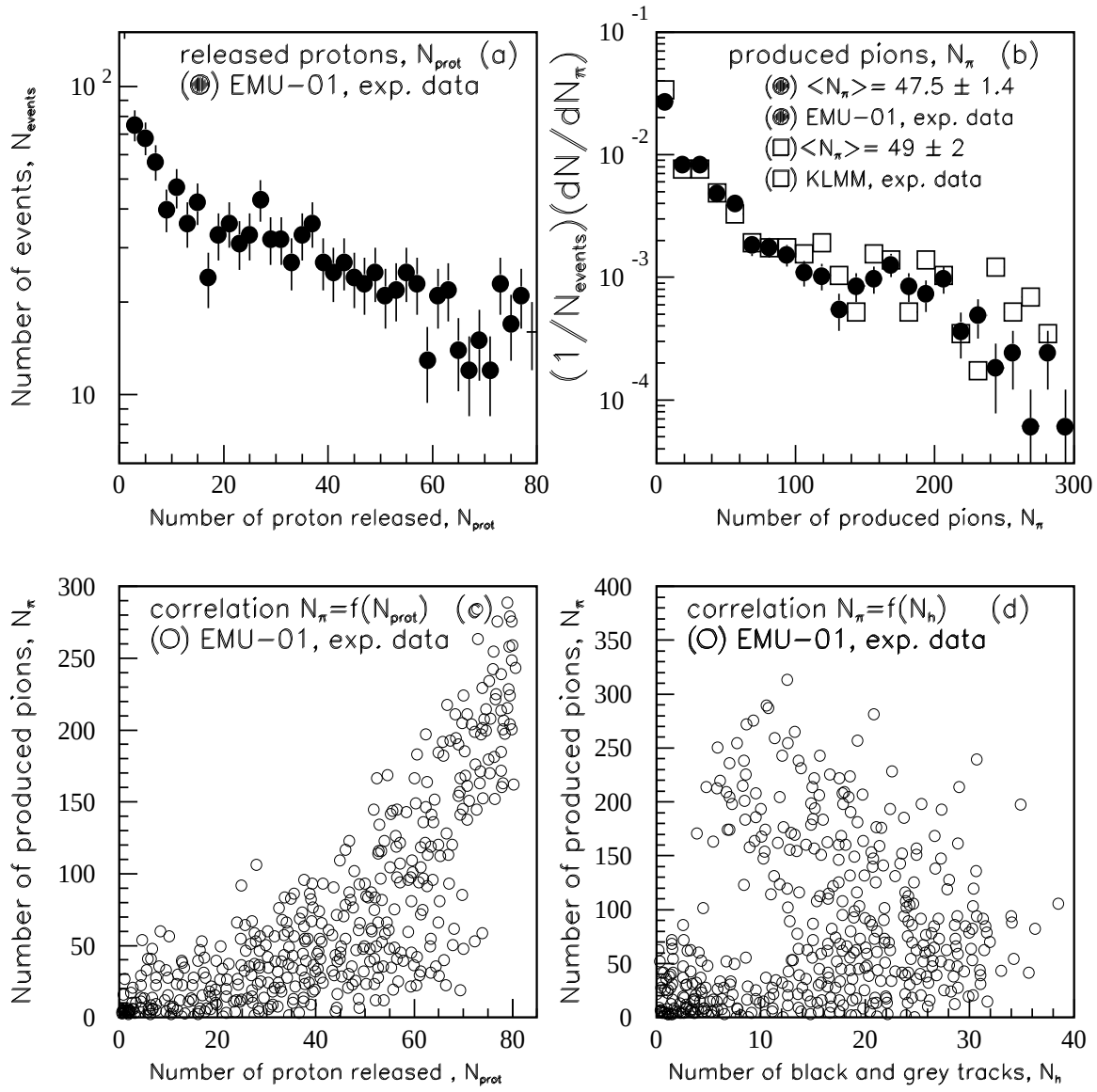

Figure 2: Part (a) - Distribution of number of proton released - full circles EMU-01 data. Part (b) - a comparison of the number of pion produced in the two experiments. EMU -01 data (full circles) ; KLMM data (open squares). Part (c) - Correlation between the number of protons released and the number of pion produced . Data from EMU-01 experiment. Part (d) - Number of pions produced as a function of the number of black and grey tracks (N_h) emitted from the target.

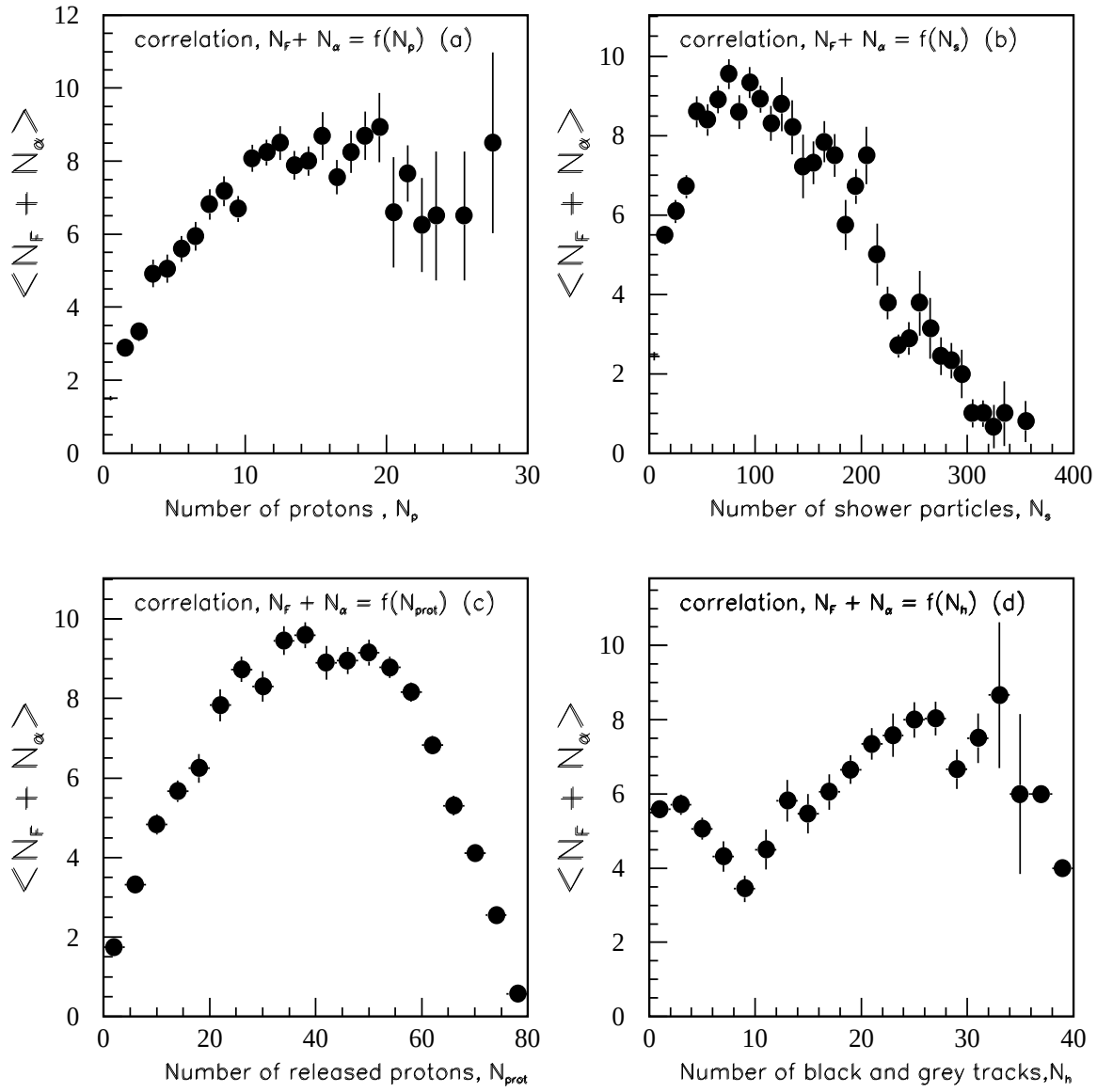

Figure 3: Correlation of mean number of alpha particles and fragments with $Z \geq 3$ ($< N_\alpha + N_F >$) with number of singly charged fragments (N_P)(Fig. 3a), with the number of shower particles (N_S) (Fig. 3b), with the number of released protons (N_{prot})(Fig. 3c) and with the number of black and grey tracks (N_h)(Fig. 3d).

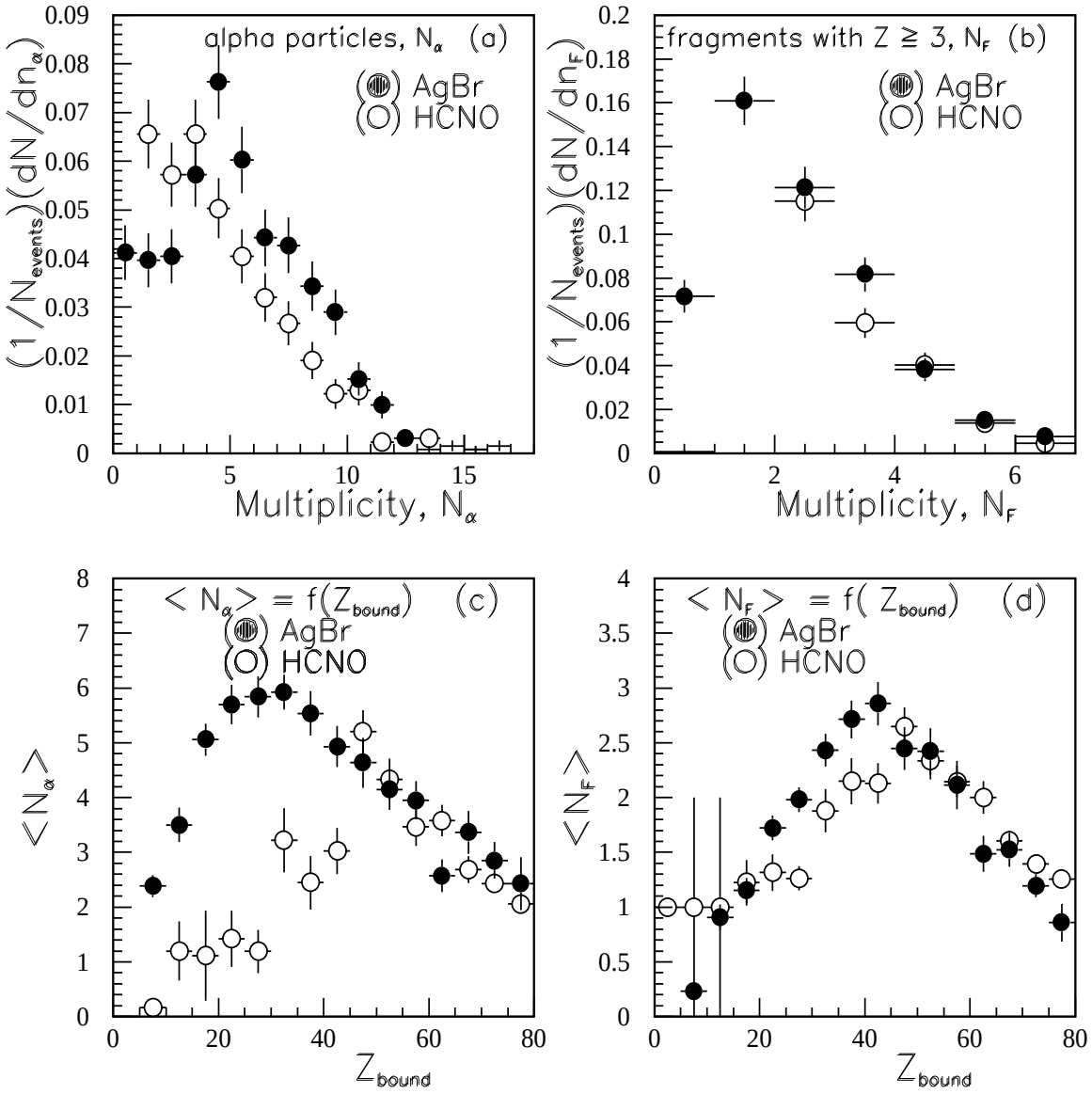

Figure 4: Part (a) - The distributions of the numbers of alpha particles in interactions with a emulsion light (HCNO) (open circles) and heavy (Ag,Br) (full circles)- EMU-01 data. Part (b) - The distributions of the numbers of fragments with $Z \geq 3$. Part (c) - The average number of alpha particles $< N_\alpha >$ as a function of Z_{bound}. Part (d) - The average numbers of fragments ($Z \geq 3$) as a function of Z_{bound}. The experimental data have the same meanings as in Part (a).

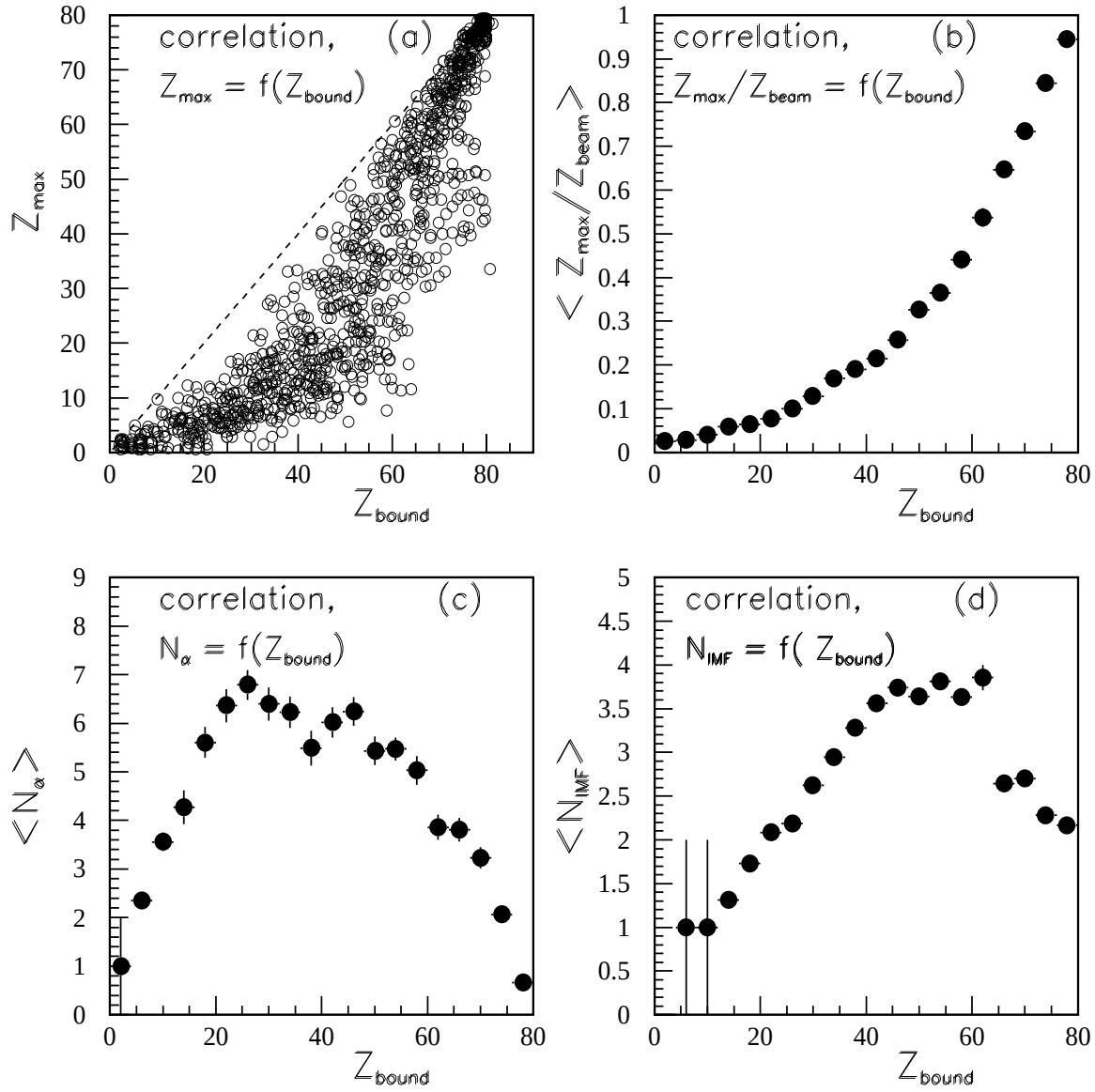

Figure 5: Part (a) - A scatter plot between the correlation of largest charge Z_{max} and Z_{bound}, in individual events . The diagonal is shown by a dashed line. Part (b) - Mean values ration $< Z_{max}/Z_{beam} >$ as a function of $< Z_{bound} >$. Part (c) - Mean numbers $< N_\alpha >$ as a function of $< Z_{bound} >$ for full sample. Part (d) - Mean numbers of intermediate fragments (IMF's) $< N_{IMF} >$ (with $3 \leq Z \leq 30$) as a function of Z_{bound}.

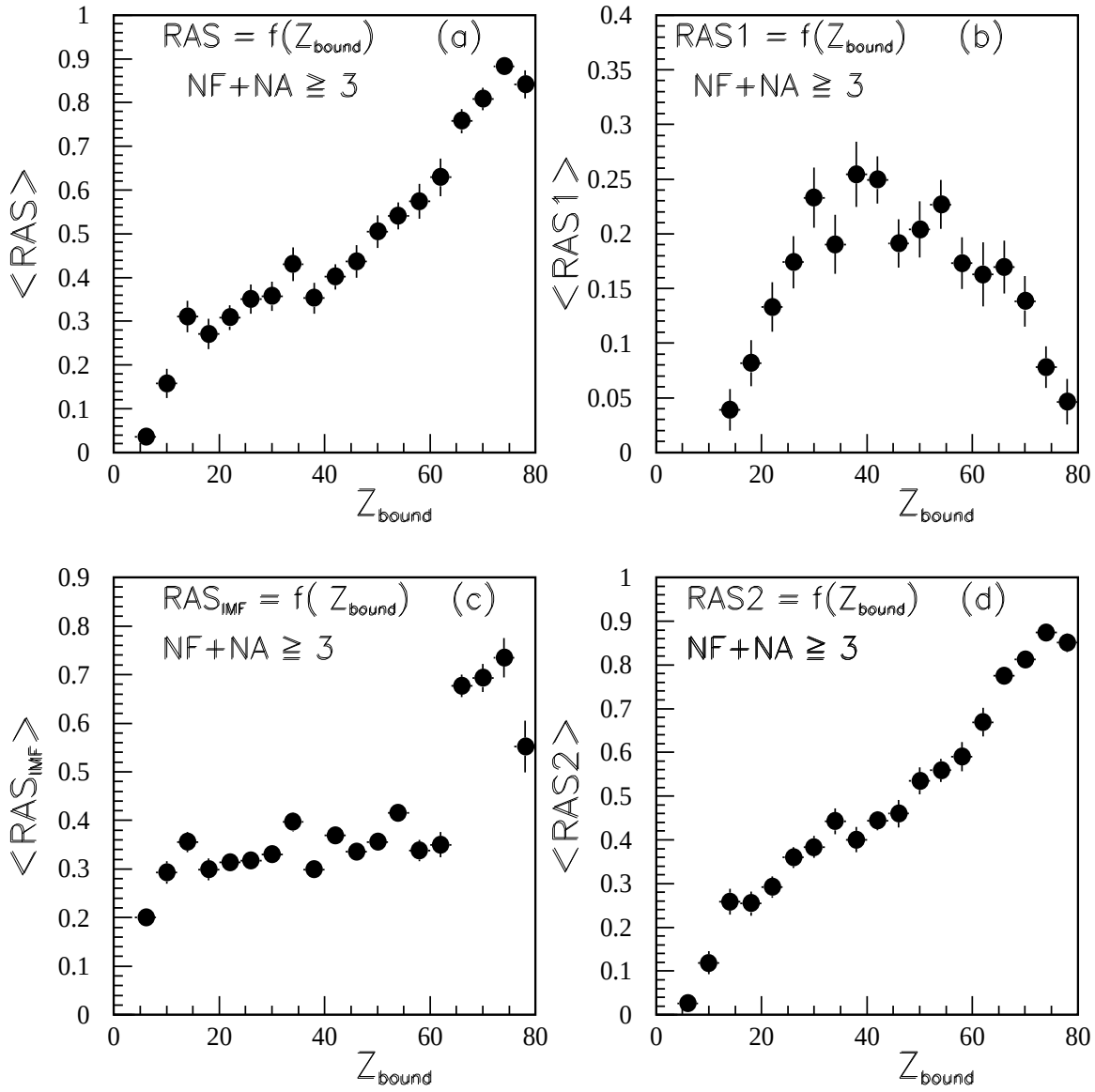

Figure 6: Part (a) - Two body relative asymmetry $< R_{AS} >$ versus Z_{bound}. Part (b)- Two body relative asymmetry $< R_{AS1} >$ versus Z_{bound}. Part (c) - Two body relative asymmetry for IMF's versus Z_{bound}. Part (d) - Three body asymmetry $< R_{AS2} >$ versus Z_{bound}. For the definitions of charged particle asymmetries $< R_{AS} >$, $< R_{AS1} >$, $< R_{AS2} >$ see section 4.2

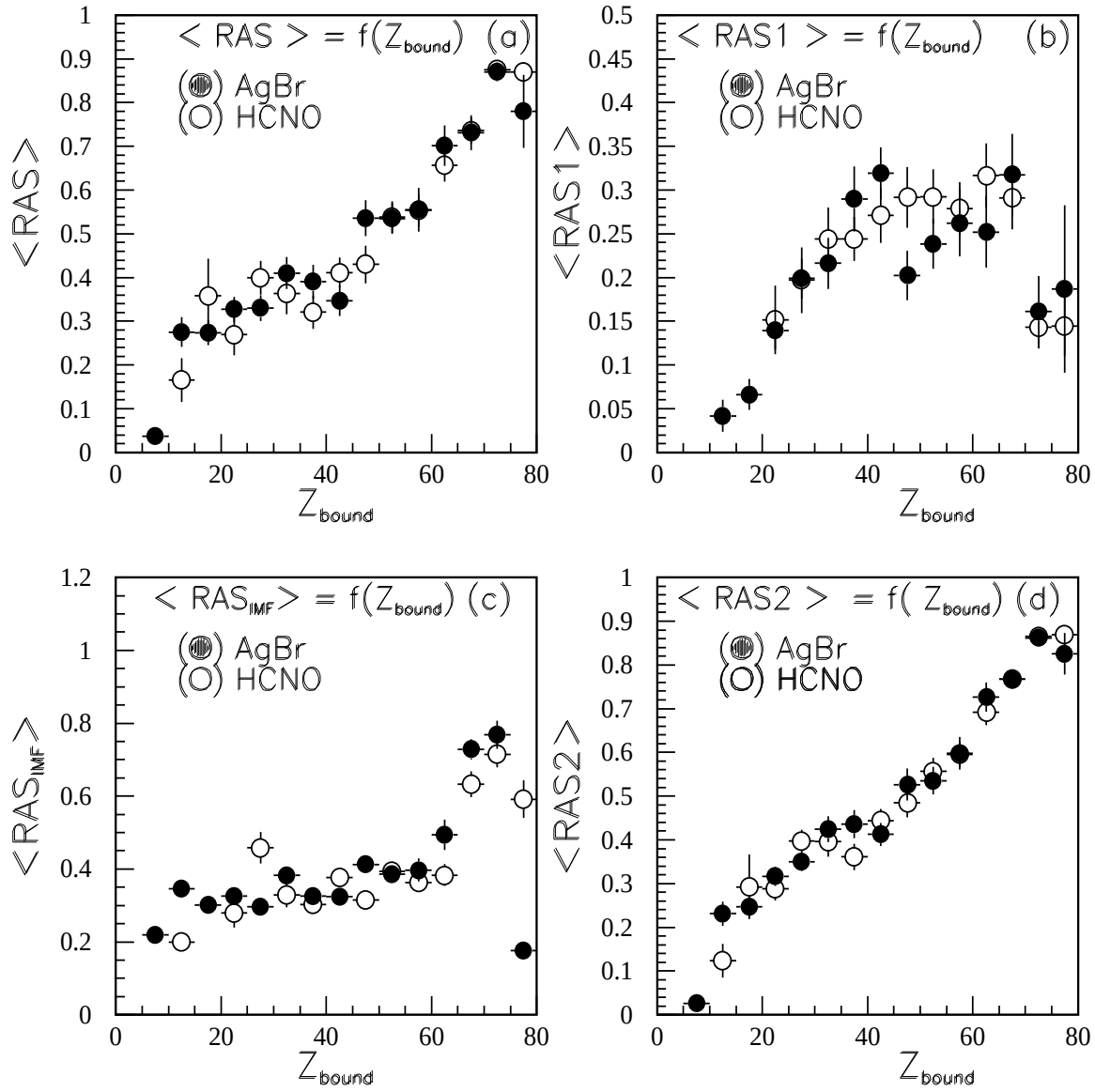

Figure 7: Part (a) - Two body relative asymmetry $< R_{AS} >$ versus Z_{bound}. Part (b)- Two body relative asymmetry $< R_{AS1} >$ versus Z_{bound}. Part (c) - Two body relative asymmetry for IMF's versus Z_{bound}. Part (d) - Three body asymmetry $< R_{AS2} >$ versus Z_{bound}. Experimental points have the same meanings as in Figure 4. For the definitions of charged particle asymmetries $< R_{AS} >$, $< R_{AS1} >$, $< R_{AS2} >$ see section 4.2.

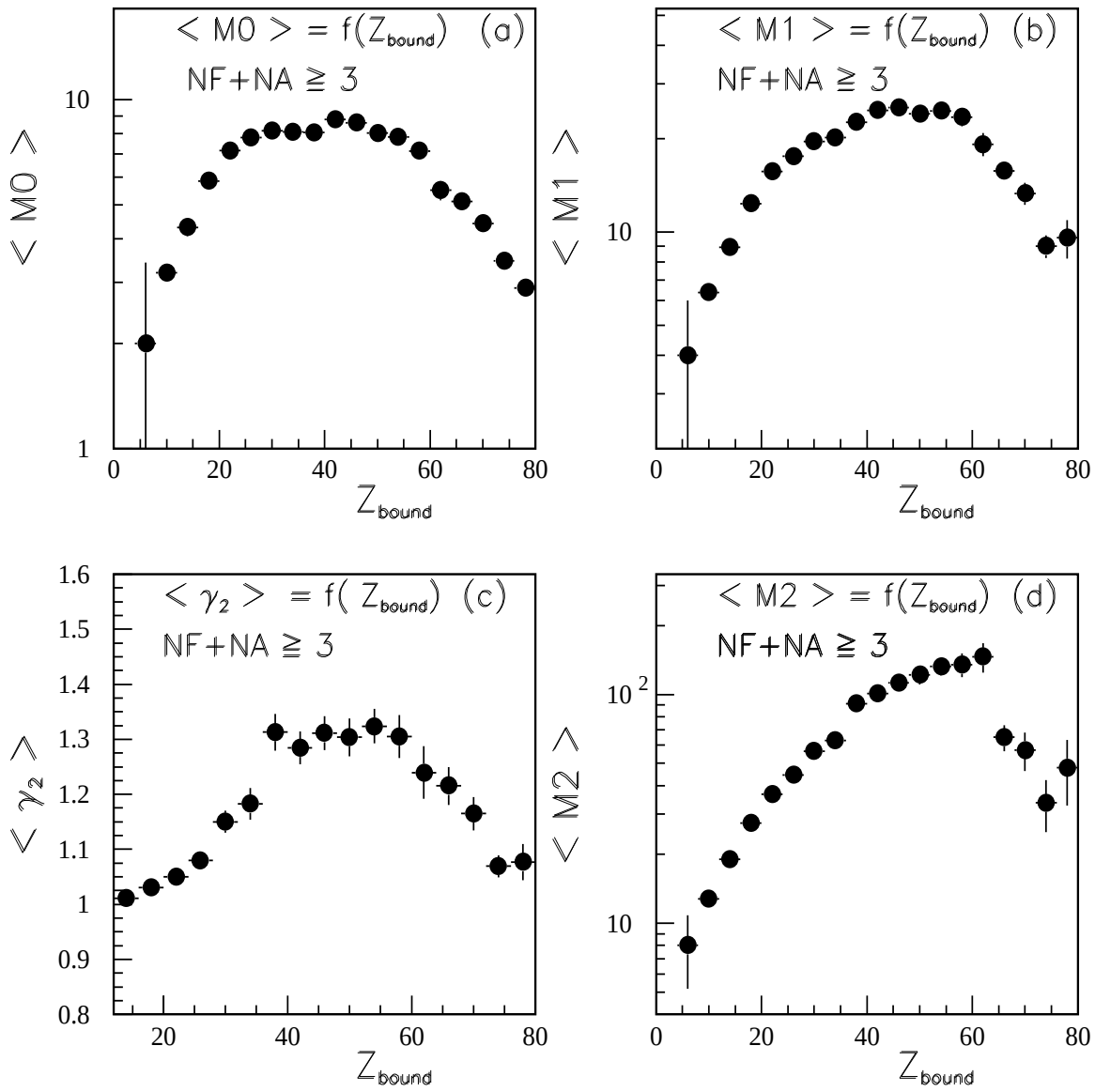

Figure 8: Mean values of zeroth moments, $< M_0 >$ (Fig. 8a), first moments, $< M_1 >$ (Fig. 8b) and second moments $< M_2 >$ (Fig. 8d) as a function of Z_{bound}. Part (c) - Variation of the mean values of the conditional moment $< \gamma_2 >$ with Z_{bound}. For the definitions see section 4.3

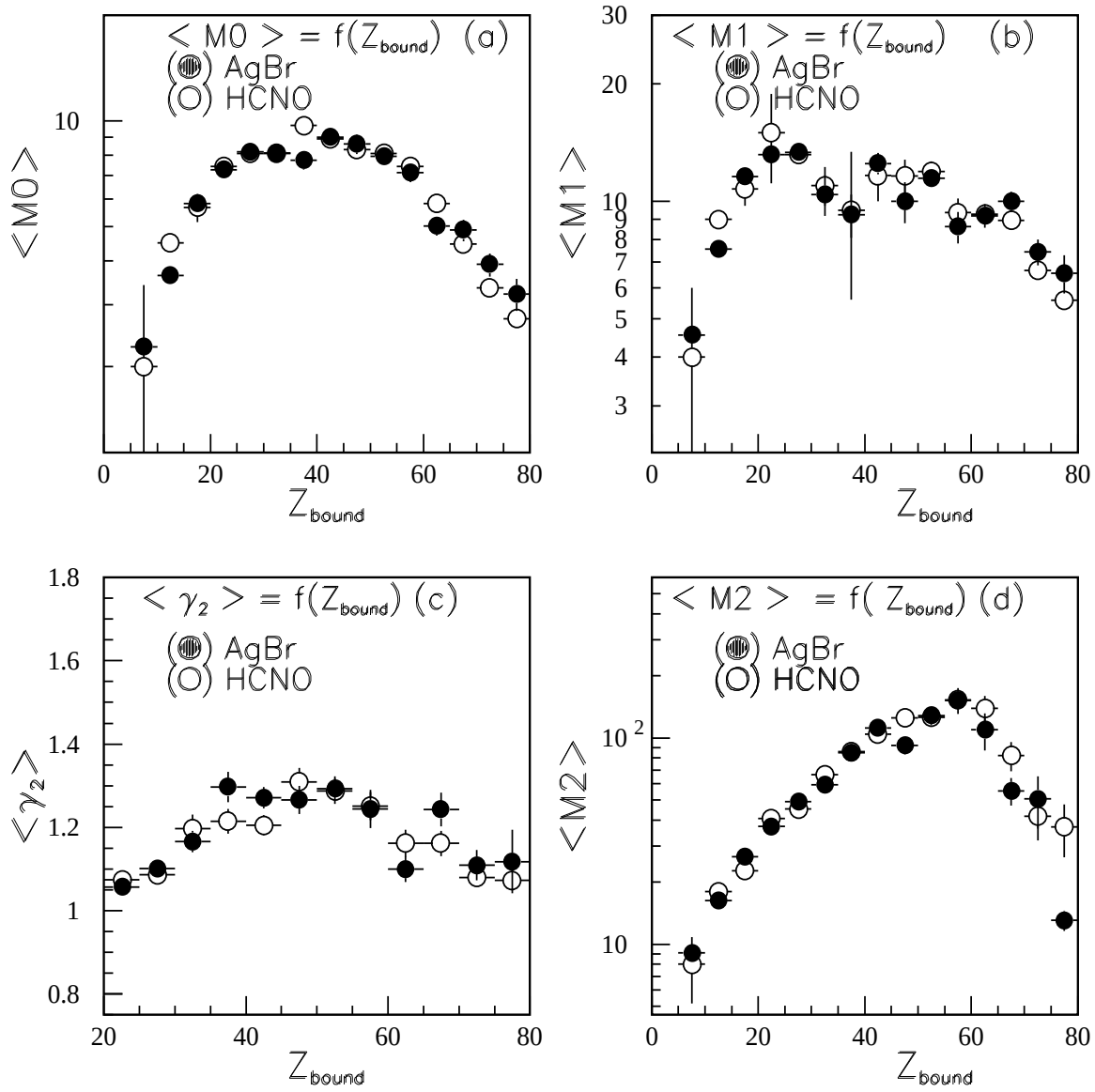

Figure 9: Mean values of zeroth moments, $< M_0 >$ (Fig. 9a), first moments, $< M_1 >$ (Fig. 9b) and second moments $< M_2 >$ (Fig. 9d) as a function of Z_{bound}. Part (c)- Variation of the mean values of the conditional moment $< \gamma_2 >$ with Z_{bound}. The experimental data points have the same meanings as in Figure 4. For the definitions of the symbols see section 4.3

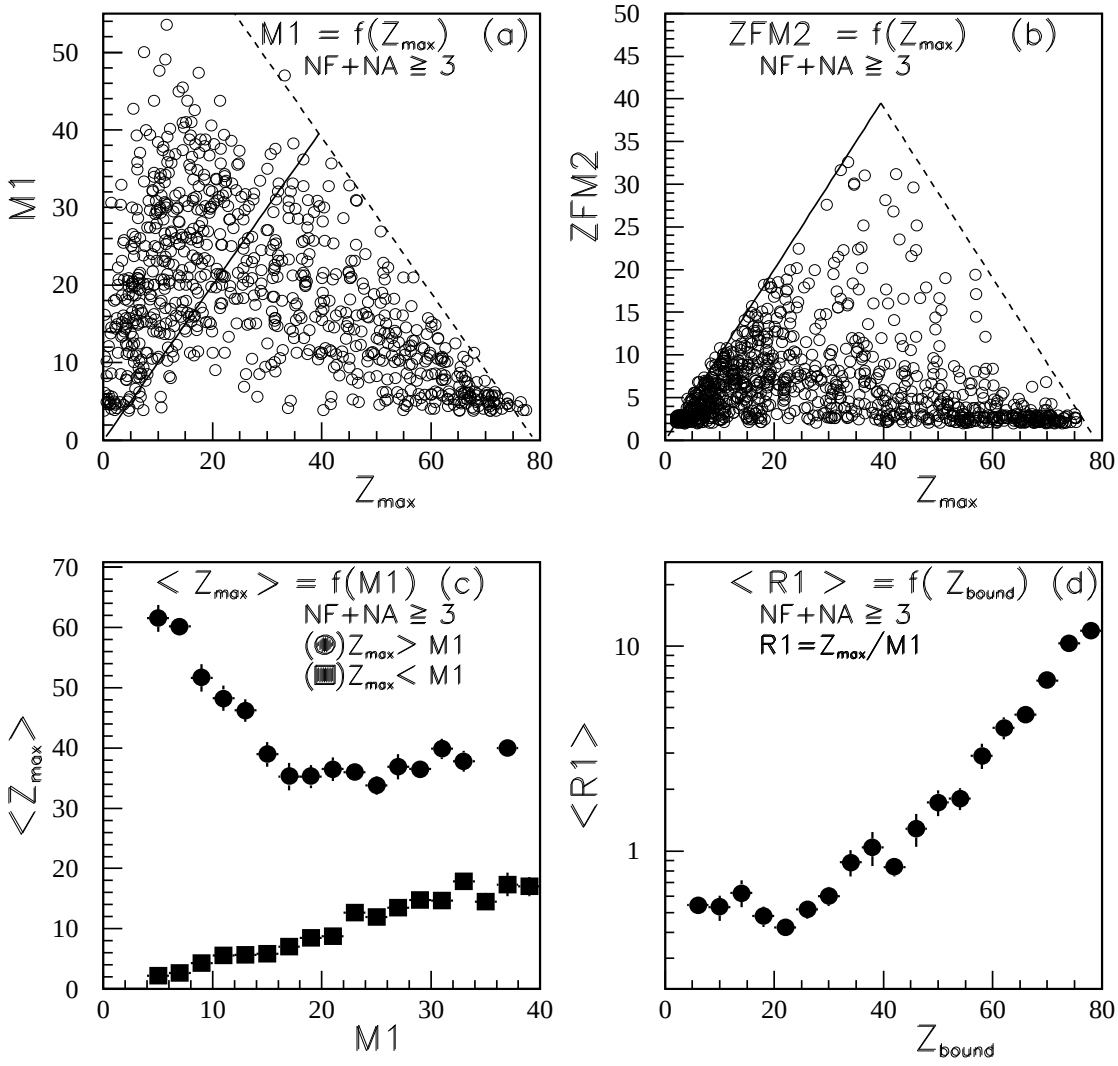

Figure 10: Part (a) - Correlation between charge on heaviest fragment Z_{max} and remaining bound charge $Z_r \equiv M_1$. Right diagonal dashed line show charge limit, left full line shows where $M_1 = Z_{max}$. Part (b) - Correlation between heaviest, Z_{max}, and second heaviest fragments. Diagonal dashed lines show charge limits, left full line shows where $Z_{FM2} = Z_{max}$. Part (c) - Mean of the charge on the heaviest fragment $< Z_{max} >$, as a function of the first moments, M_1 separated into those events where Z_{max} is greater or less than M_1. Part (d) - Mean values of the leading fragment ratio $< R_1 >= Z_{max}/M_1$ as a function of bound charge Z_{bound}.

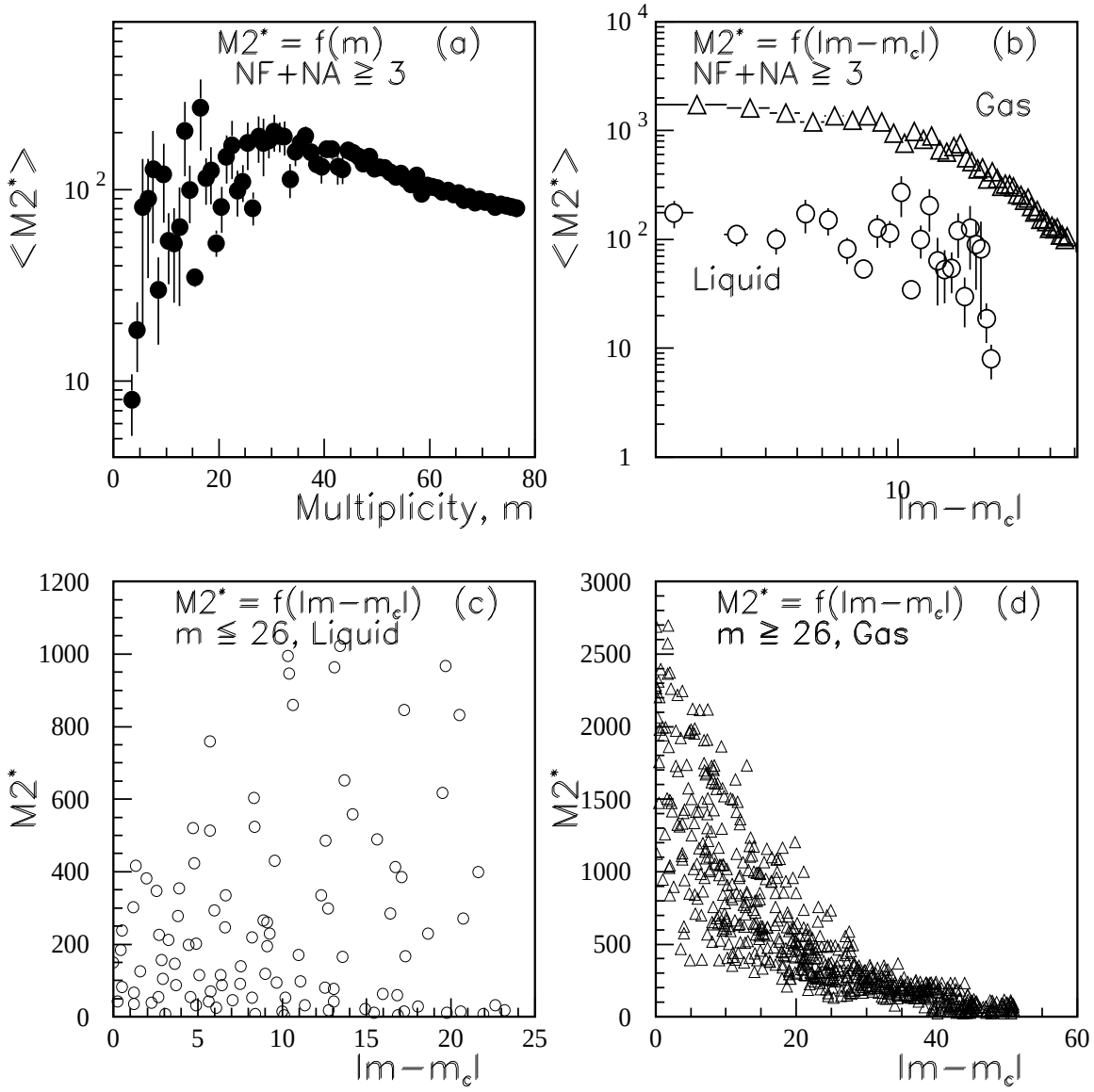

Figure 11: Part (a) - Mean second moments $< M_2^* >$ as a function of multiplicity m. Part (b) - Mean second moments $< M_2^* >$ as a function of the multiplicity difference ζ assuming $m_c = 26$. Part (c) - A scatter plot of second moments M_2^* as a function of of the multiplicity difference ζ for liquid phase. Part (d) - A scatter plot of second moments M_2^* as a function of of the multiplicity difference $|\zeta|$ for gas phase.

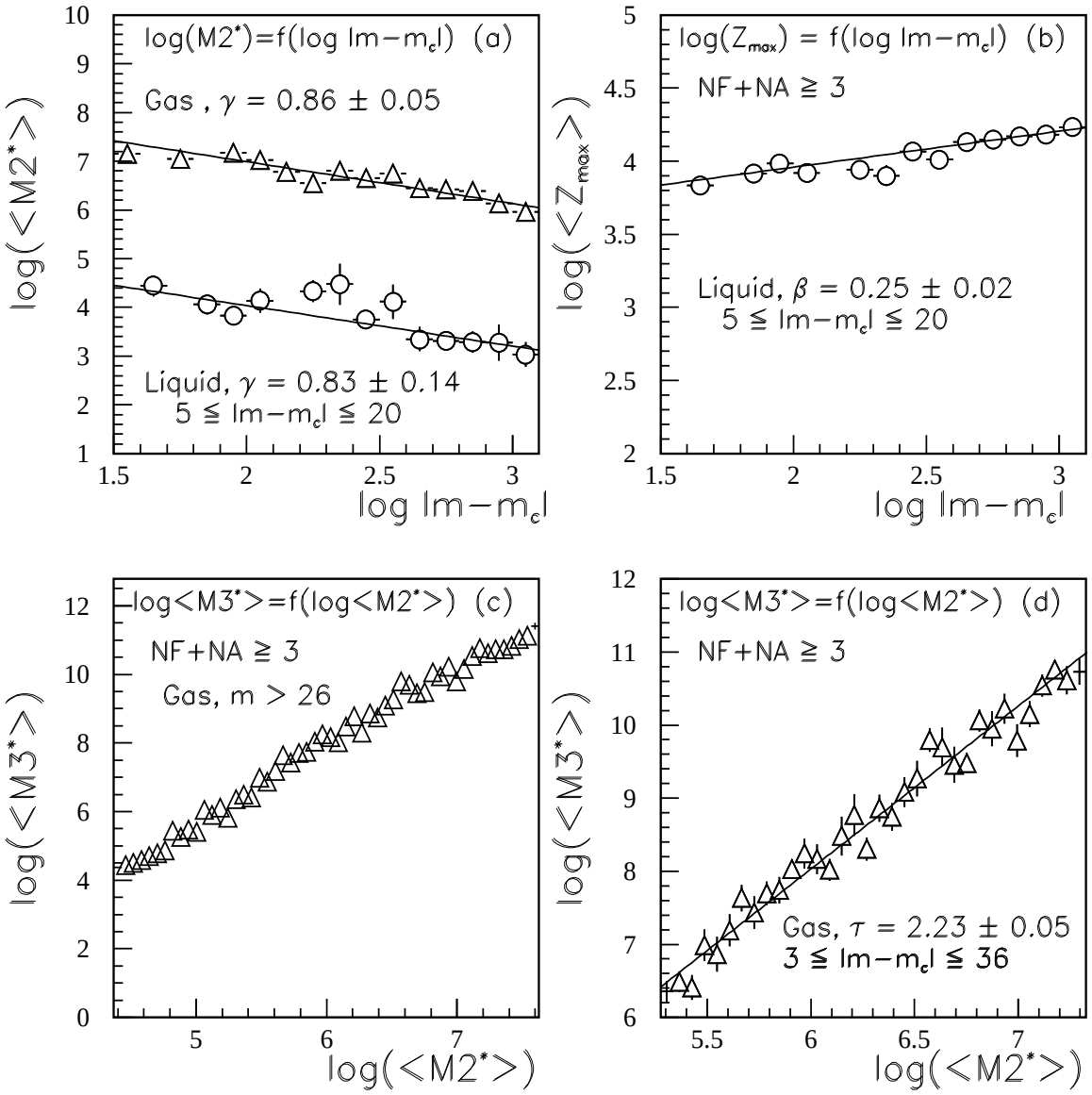

Figure 12: Part (a) - A log-log plot of mean second moments $< M_2^* >$ as a function of multiplicity difference ζ assuming $m_c = 26$, over a limited range of ζ. Linear fits are shown for both the gas and liquid phases to define the exponent γ (see Eq. 13). Part (b) - A log-log plot of the mean values of heaviest charge, $< Z_{max} >$, as a function of multiplicity difference ζ, in the liquid phase, assuming $m_c = 26$. A linear fit is shown to define the exponent β, Eq. 14. Part (c) - Correlation between mean second and third moments $< M_2^* >$ and $< M_3^* >$, for the gas phase, assuming $m_c = 26$. Part (d) - A log - log plot for correlation between mean second and third moments $< M_2^* >$ and $< M_3^* >$, for the gas phase, assuming $m_c = 26$ over a limited range of ζ. A linear fit is shown to define the exponent τ, Eq. 15.